

CHARACTERIZATION OF A UWB TRANSCEIVER FOR MINING APPLICATIONS

Michael Edgar¹, Jonathan Aw¹, John Dudley¹, Roger Marley¹, Anthony Reid¹, Zane Smith¹
Adrian Taylor¹ and Ross McAree¹

ABSTRACT

Ultra wideband (UWB) transceivers have become available relatively recently for use in high accuracy Real Time Location Systems (RTLS). They have potential for locating and tracking people and equipment in mining contexts. These devices operate in an unlicensed region of the microwave spectrum; from 3-10 GHz. Range is measured between a pair of transceivers and resolutions of the order of millimetres have been achieved. We describe the advantages of these systems and present measurements obtained with a commercially available transceiver.

INTRODUCTION

Locating people and equipment is of vital importance in mining automation systems. This paper discusses the benefits of ranging with Ultra Wideband (UWB) devices, a class of technology that shows promise for this application and presents a performance evaluation of a commercially available UWB system.

Transceivers

The UWB systems we discuss are transceiver based. A transceiver is a combined transmitter and receiver that generates a reply signal on receipt of an incoming signal. These devices are also known as transponders. There are many types of wireless transceivers; Radio Frequency Identification (RFID) tags are the most common. The major advantage of transceivers is that they are active: they generate and transmit return signals, rather just a passive reflection of the incoming signal, as in non-cooperative, passive, ranging techniques such as RADAR or Light Detection and Ranging (LiDAR).

A benefit of transceivers over purely passive reflection based systems is the potential for higher Signal to Noise Ratios (SNR) than passive systems. The amplitude of the return signal will have a range, r , dependence of r^{-2} , as opposed to r^{-4} for an uncollimated, passive system. This amplitude will also be totally independent of the reflectivity of the illuminated surface.

The position of the transceiver can be accurately determined, so the precise location of the source of the return signal is always known. In a passive system, the location of the region with the peak amplitude return will vary considerably with conditions and orientation of the illuminated object. This is particularly true for an object with a complicated geometry, such as a vehicle.

The true advantage of transceiver based systems is that the amplitude and location of the returned signal are defined solely by the transceiver itself. The properties of that signal are completely independent of the surface properties, geometry and orientation of the object on which they are mounted. This makes these devices particularly attractive where the position and orientation of objects is required to a specific accuracy and precision.

¹ CRCMining, The University of Queensland, St. Lucia, Qld., 4072
Proceedings of the 2012 Australian Mining Technology Conference
8-10 October, 2012, Perth, Western Australia, pp. 125-140.

Ultra Wideband Impulse Radios

Figure 1 shows the signal characteristics of an Ultra Wideband (UWB) system. The generation of short pulses in the time domain produces a large bandwidth in the frequency domain. In UWB systems, the pulse widths are of the order of nanoseconds and the associated bandwidths of the order of GHz

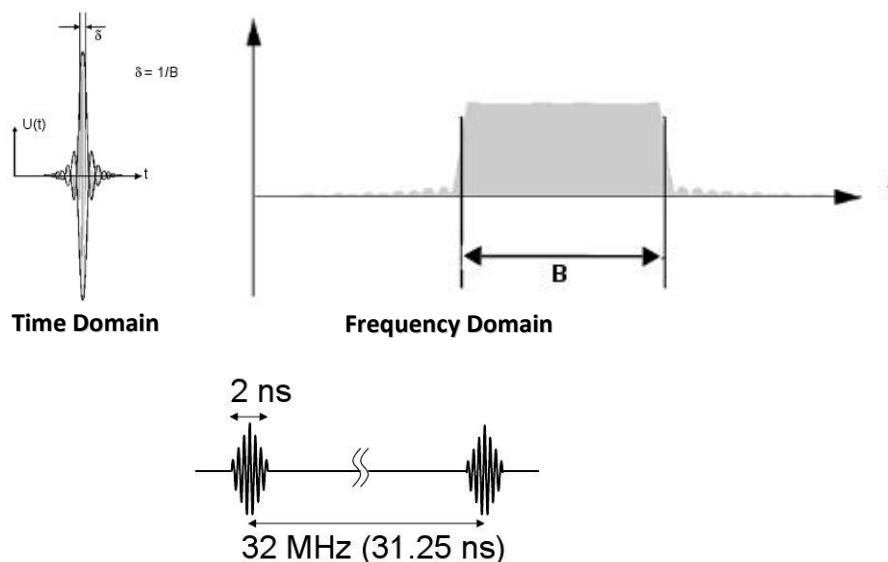


Figure 1. The basic features of an UWB Impulse Radio. The top image shows the Fourier conjugates, the sinc pulse and the square function. Due to the inverse nature of the Fourier transform, a sinc pulse with a pulse width $1/B$ seconds in the time domain, corresponds to a square pulse with a bandwidth of approximately B Hz, in the frequency domain (Nanotron, 2007). Shorter pulses correspond to broader bandwidths. The lower image shows an example of the time series for a proposed Hitachi UWB IR (Nakagawa *et al.*, 2009).

The type of UWB transceiver used in precision ranging is often referred to as an UWB Impulse Radio (UWB IR). Unlike conventional radios, UWB IRs do not produce a modulated carrier wave. A UWB IR produces a time series of very short, impulse like pulses. They typically have a Pulse Repetition Frequency (PRF) of order 10 MHz, yielding a duty cycle of only a few percent. As the output is a time series of short pulses, these UWB methods are often referred to as time domain techniques.

Regulations

Sahinoglu *et al.* (2008) discuss the regulations and standards for UWB systems in detail. In 2002, the US Federal Communications Commission (FCC) authorized the unlicensed use of UWB systems in the frequency range from 3.1 to 10.6 GHz. The FCC power spectral density emission limit for UWB transmitters is -41.3 dBm/MHz. This has been the basis for the power limits of UWB systems, although there is some international variation, e.g. Europe.

Both the FCC and the International Communications Union, Radiocommunications Sector (ITU-R) now define UWB systems as having a bandwidth of at least 500 MHz or a fractional bandwidth greater than 20% .

UWB IR Advantages

The physical nature of the UWB pulse itself provides several advantages for a precision ranging system over a narrow band wireless system. These are described in detail elsewhere (Sahinoglu *et al.*, 2008 and Miller, 2003). The most relevant advantages for precision ranging are summarized below.

Resolution

In estimation theory and statistics, the Cramer-Rao Lower Bound (CRLB) is the minimum variance for any unbiased estimator. For ranging (Kay, 1993), the CRLB defines the minimum standard deviation as:

$$\sigma = (B_{eff}\sqrt{SNR})^{-1} , \quad 1$$

where B_{eff} is the effective bandwidth. Therefore, increasing the bandwidth is a much more efficient method of improving ranging resolution than increasing the amplitude of the signal.

Multipath Resistance

One of the most important advantages of UWB systems is their resistance to multipath effects. Due to reflections off surrounding objects, signals propagate to a receiver by different routes, arriving at different times and may interfere with each other. This is well known problem in most radio ranging and localization systems, including GPS. As the UWB pulses are very short in time, their physical length is also quite short, i.e. a 1 ns pulse corresponds to a pulse length of 30 cm. Ideally, objects further away than half the length of the pulse cannot cause interference at the receiver. As a result, UWB systems are being used extensively for precision ranging in indoor applications, where many reflective surfaces are present.

Resistance to Jamming and Interference

Processing gain, G_p , is a concept used in spread spectrum (Maxim, 2003) and UWB IR systems. It is a measure of the resistance that these two types of systems have to interference from other narrow band signal sources. In UWB IR, it can be shown that G_p is simply the inverse of the duty cycle (Gezici *et al.*, 2007). A UWB IR with a duty cycle of 1%, would have a 100 times greater resistance to interference than a narrow band system.

Low Probability of Interference with Other Radio Systems

As UWB systems spread the energy of their signals over a wide bandwidth, the resultant peak amplitude is greatly reduced, the total radiated power divided by a factor of G_p . When the FCC and the ITU-R developed the regulations for UWB systems, the power levels were chosen to be below naturally occurring noise floors in the frequency band (see Molisch, 2006). It is unlikely that a UWB system could be detected by, let alone interfere with, a narrow band system.

Resistance to Environmental Attenuation

All signals in the 3-10 GHz range suffer very low attenuation when exposed to environmental effects such as rain or dust. Even at a heavy rainfall rate of 100 mm/hr, the attenuation at 10 GHz is only 1 dB/km (Olsen, 1978). The attenuation during a severe dust storm has been calculated as 0.5 dB/km at 10 GHz and only 0.1 dB/km at 3 GHz (Goldhirsh, 2001).

RANGING CHARACTERIZATION

Hardware

There are a number of commercially available UWB systems. At least four of these have measured resolutions of 0.5 m or less.

1) Nanotron uses a Chirp Spread Spectrum method to produce an 80 MHz bandwidth at 2.4 GHz (Nanotron, 2011). Their system is capable of using two-way Time of Flight (ToF) or Time Difference of Arrival (TDoA) ranging. Although this is not truly a UWB system, it has 80 MHz bandwidth, it is included in IEEE 802.15.4a, the standard governing UWB ranging systems (Shaninoglu *et al.*, 2008). Rommel and Haich (2009) present measured resolution values of 50 cm.

2) The Ubisense Series 7000 is a UWB system with a 2 GHz bandwidth centred at 7 GHz (Ubisense, 2011). It uses Angle of Arrival (AoA) and/or TDoA ranging. The manufacturer claims an accuracy of 15 cm. Zhang *et al.* (2011) have measured resolutions of 20 cm and Cho *et al.* (2010), state the resolution was 10 cm. Zhang *et al.* also tested the system as a pose estimator for a crane.

3) Zebra Dart has a system with a 400 MHz bandwidth centred at 6.55 GHz and uses TDoA ranging (Zebra Technologies, 2011). Although this falls short of the 500 MHz bandwidth definition of a UWB system, the principles of operation are identical. This was previously the Multispectral Solutions Dart system with which McGoughan, (2009) measured a minimum resolution of 8 cm.

These three systems described have the typical RFID architecture, a more sophisticated receiver, or anchor, carrying out ranging measurements to a simpler tag (see Rommel and Haich, 2009).

4) Multiple authors have measured resolutions of order 3 cm for Time Domain's P210 transceiver (McGoughan, 2009, Park *et al.*, 2008, Richardson and Shan, 2009). Unlike the previous three systems, the Time Domain system carries out ranging between two identical transceivers.

We choose to evaluate the Time Domain system due to its significantly higher resolution, as well as the ability to vary its configuration, as discussed below.

Time Domain PulsON P400 RCM

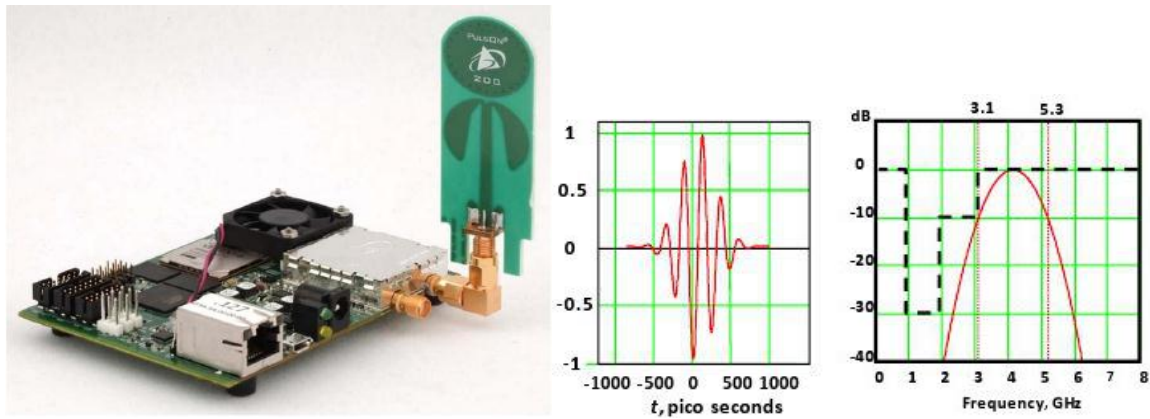


Figure 2. The Time DomainP400 RCM. The left image shows the RCM, the dimensions of the board are 10.5x 7.7 x 2.2 cm. The green object is the BroadSpec omin-directional antenna, Schantz (2003). The graphs on the right show the outgoing pulse from the transceiver and the associated bandwidth. The dotted line in the bandwidth plot shows the FCC relative power emission limits. The bandpass of the transceiver has been filtered to meet these power limits.

Figure 2 shows the PulsON P400 Ranging and Communications Module (RCM) (Time Domain, 2011), which is a replacement for the P210. It has a 3.1-5.3 GHz bandwidth at -10 dB, giving a fractional bandwidth of 48%. It uses two way ToF ranging (Dewberry and Beeler, 2012), measuring the time of arrival of the leading edge of the UWB pulse. In order to accurately measure the ToF, the RCMs directly scan and analyse the received pulse waveform. They also have the capability for the real-time display and storage of this waveform, see Figure 8. With this feature, a great deal of information about the quality of the range measurement can be determined and it is most useful for initial configuration, setup and trouble shooting.

This system is a coherent system which gives it a significant advantage over other commercial systems. This allows individual pulses to be summed together, increasing both SNR and G_p . By default, the system averages 128 pulses together. The nominal PRF for the system is 10 MHz, corresponding to a duty cycle of approximately 1%. Averaging over 128 pulses, increases G_p to 41 dB. The amount of averaging can be varied by factors of two, trading SNR for speed. With averaging of 512 pulses, we have successfully made measurements at ranges up to 160 m.

The default gain of the system corresponds to the peak emission power permitted under the FCC/ITU-R rules. There is a capability to increase this gain, for experimental reasons only, by up to 14.5 dB.

The antenna has a standard SMA connector and is detachable. Coaxial cables may be used to mount the antenna remotely from the transceiver itself. Calibration over a known distance allows removal of the propagation delay due to the cable. The transceivers are calibrated at the factory to allow for the default configuration, in which the antenna is connected to the transceiver board via a single 90° SMA adapter, see Figure 2. We have successfully run a transceiver with 10 m of LMR300 coaxial cable and removed the propagation delay, although it does produce significant attenuation, particularly at the high frequency end of the bandpass.

Method

All the data presented in this section were obtained under conditions as shown in Figure 3. The default averaging of 128 pulses was used for all measurements. With this averaging, a complete ranging measurement between two transceivers typically took 42 ms. Data was obtained at 10 Hz. The default gain and antenna configuration, as shown in Figure 2, were used. For weatherproofing, both transceivers were mounted in polycarbonate enclosures, as shown in Figure 10.

A series of 22 measurements sets were made at 12 ranges from 5 to 50 m, over two days. The weather was fine on both days, as in Figure 3. Data was acquired without the polycarbonate lid mounted at all twelve ranges on the first day. Measurements were repeated without the lid at 10, 20 and 40 m on the second day. Measurements with the polycarbonate lid mounted were also repeated at 10, 20, 30, 35 and 40 m on the first day.

Resolution

Figure 4 shows histograms of the ranging measurements at two ranges. Both show standard deviations of the order of 3 cm. While the histogram at the shorter range is Gaussian in form, the result at 50 m has a marked negative skew.

Figure 5 presents a summary of the resolution of the measured data sets and the skewness of the histograms. At short ranges, the resolution can be as low as 2 cm increasing to approximately 3.5 cm at 20 m. These levels of resolution are consistent with those measured for the earlier P210 (McGoughan, 2009, Park *et al.*, 2008, Richardson and Shan, 2009).

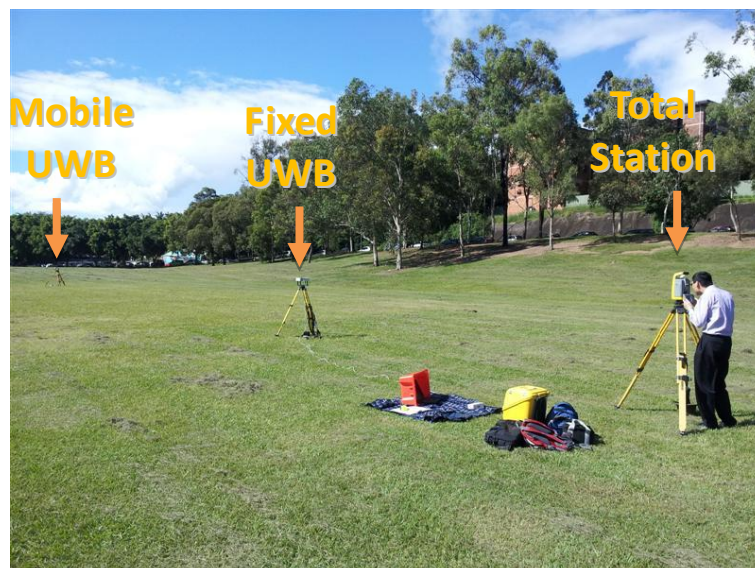


Figure 3. The typical experimental setup for measuring ranging performance. Measurements were made in a soccer field adjacent to the University of Queensland. The Fixed and Mobile UWB devices were identical P400 RCMs, both mounted on tripods. The position of one transceiver was kept fixed, while the other was moved. The positions of the antenna phase centres were surveyed for each RCM, at each separation.

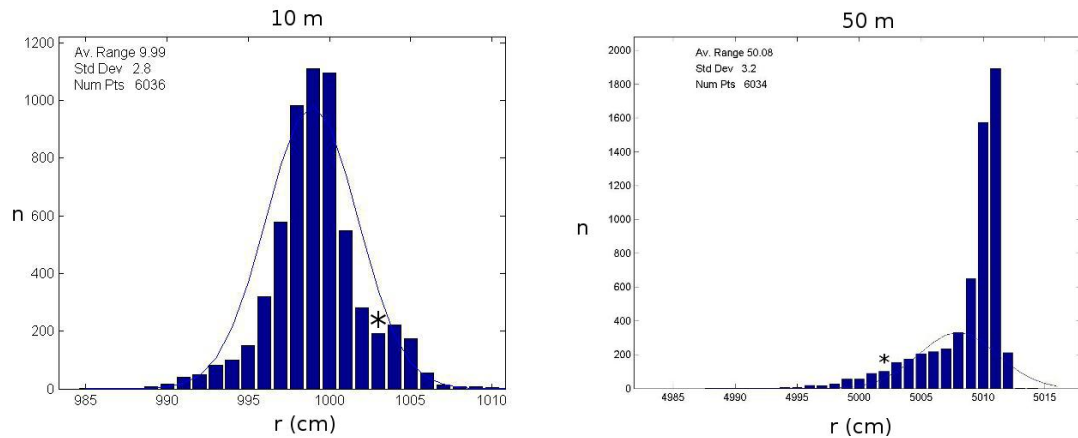


Figure 4. Ranging measurements at nominal ranges of 10 and 50 m. The asterisk visible in the figures shows the position of the range as determined by surveying. The solid line represents a Gaussian, with the measured standard deviation and a peak value equal to the number of counts within the bin within which the mean of the distribution lies. The bins are 1 cm wide for both images. The size of these data sets is typical of all the sets.

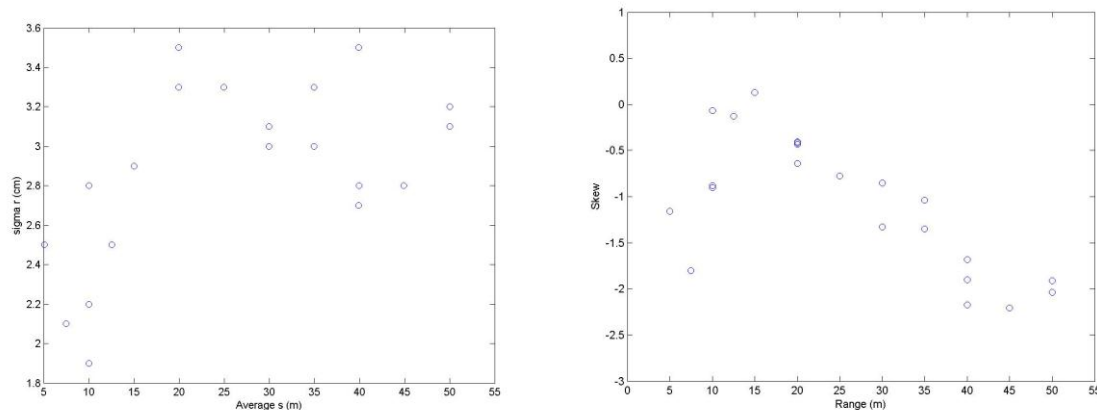


Figure 5. The resolution and skewness of the measurements. The left figure shows the calculated standard deviations for the 22 histograms obtained for the individual measurements in cm versus the surveyed separation, s , between the antennas on the two transceivers. The figure on the right shows the variation in skewness of the histograms with this range.

The negative skewness is pronounced at very short ranges and increases systematically at ranges longer than approximately 15 m. The manufacturer states most of their testing and calibration was carried out in the 10 to 30 m range. The increase in skewness at short ranges is believed to be due to saturation. Longer ranges will produce lower SNR values, reducing resolution and increasing the probability that the ToF algorithm will falsely detect the leading edge of the pulse in the noise that precedes the actual pulse. This produces a higher percentage of short range measurements with increasing range (Dewberry, 2012).

Accuracy

Figure 6 shows the range bias for all 22 data sets. This is the variation of the accuracy of the range measurement with range. Park *et al.* (2008) measured similar behaviour for the earlier P210. The range bias is evident as an increasing distance between the mean of the range measurement distributions and the surveyed distance with increasing range. This is shown in Figure 7, containing all the individual range measurements from the 22 data sets. The manufacturer states the calibration for the antenna propagation delay is typically carried out at

a range of ≈ 20 m, which explains the low range bias at this distance (Dewberry, 2012). When the individual range measurements are examined rather than the averages, the ranging accuracy is quite good. Approximately 97.7 % of measurements are with ± 10 cm of the surveyed distance. Only 0.14% of the measurements have a difference > 15 cm. The range bias reduces the effect of the large number of short range measurements present in distributions with negative skews.

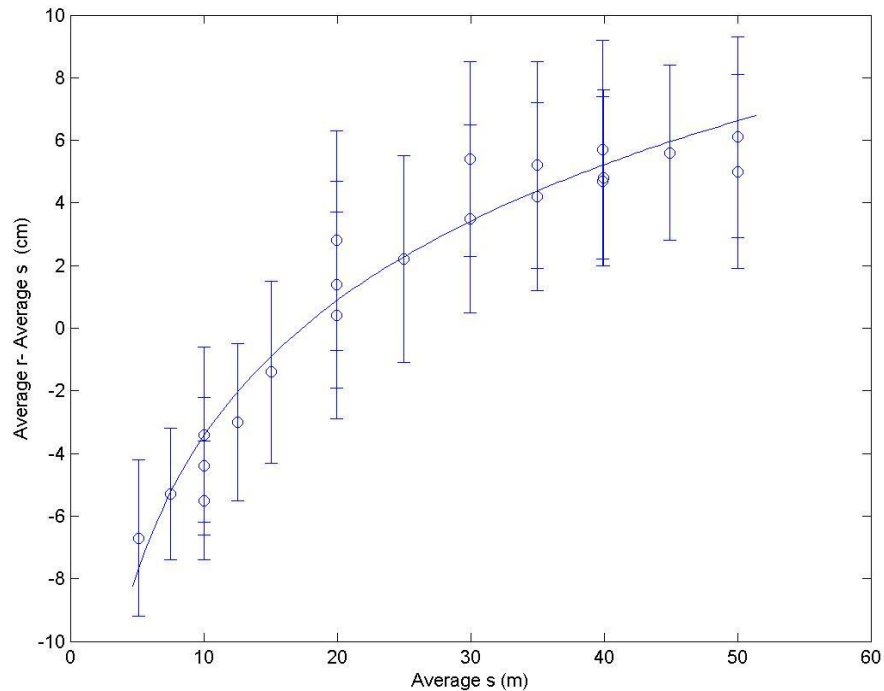


Figure 6. The range bias for the measured mean range. The circles in the figure represent the difference from the mean range as determined from the measured histograms, r , and the surveyed distance between the two antennas, s . The error bars represent $\pm 1 \sigma$. It clearly shows that there is a systematic range bias for the mean as calculated from the histograms. The equation of the solid line is given by $r-s = 0.14\log(s) - 0.18$ m. The figure also shows that all of the repeated measurements, i.e. with and without the polycarbonate lid and on successive days, lie within 1σ of each other.

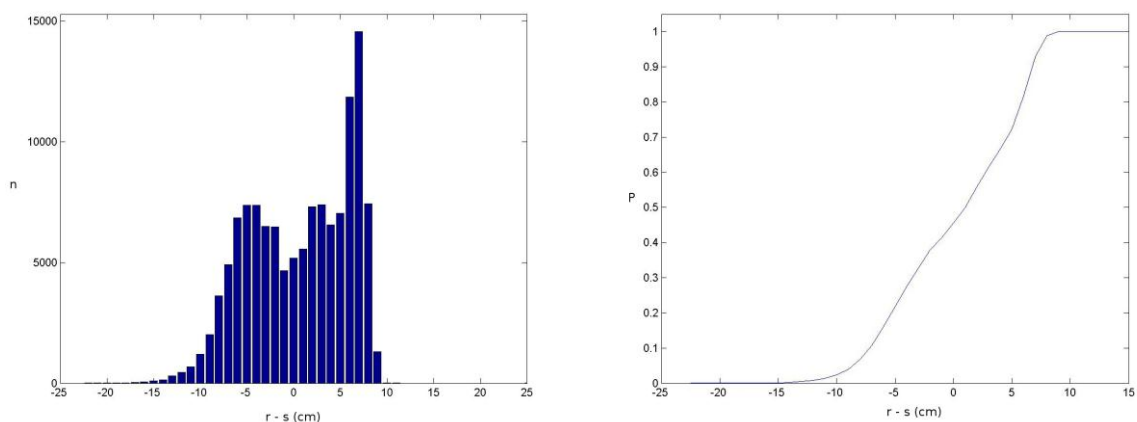


Figure 7. The merged histogram of the 22 data sets. The figure on the left shows the combined histogram of all the 22 data sets for the difference, $r-s$, between the UWB measured range, r , and the surveyed separation, s . It includes 126,875 individual ranging measurements. No corrections have been made to the data other than subtracting s . The left image shows the cumulative probability distribution for the histogram.

REFLECTIONS

UWB systems have the potential to be highly resistant to reflections and multipath effects. In this section, we present measurements made in the presence of reflections.

Waveform Measurements

Figure 8 shows examples of the received waveforms under two very different conditions. The multiple reflections present in the laboratory are immediately apparent. However, as the pulse lengths are so short, most of the reflections do not interfere with the leading edge of the pulse. The system still returns reliable ranges. Figure 13 shows examples of histograms for ranging measurements made in the same laboratory environment. Although, these systems are resistant to multipath effects, they are not immune. The range between transceivers was only approximately 4.5 m, however, the standard deviations of approximately 3.5 cm are typical of measurements obtained at ranges of greater than 20 m in the soccer field.

Figure 9 shows the received waveforms obtained in a simulated mining environment. As expected, the level of reflections lies between the soccer field and the lab environment. In most instances the level of reflections is minimal. However, as the orientation of the vehicles is varied, reflections may occur off various parts of the vehicles' structures. Provided care is taken in choosing the location and mounting of the transceivers, reflections and multipathing are unlikely to be a significant problem in a mining environment.

Measurements with Reflectors in Close Proximity

Figure 10 shows the configuration of transceivers for evaluating their performance in close proximity to reflectors. These were measured at three separate ranges. The experimental setup was the same as shown in Figure 3. All of the measurements with the reflectors were made on the second day of the experiment. The results are presented in Figure 11 and show there is no statistically significant difference in the behavior between the measurements obtained with and without the reflectors in place.

As the transceiver measures the arrival time of the leading edge of the pulse, reliable ranging measurements can be made as long as the signal from the first reflection arrives more than approximately 0.5 ns, i.e. the first half of a pulse, after the direct line of sight signal.

ENCLOSURES

Figure 12 shows the transceiver mounted in Al, hermetic enclosures intended for field deployment. The antenna requires a separate dielectric enclosure for protection. While the low loss properties of Teflon at microwave frequencies are well known, there are significant practical difficulties; it is expensive, difficult to machine, cold flows and it is difficult to obtain a good O-ring seal with. While not as low loss as Teflon or high-density polyethylene, Delrin (Acetal homopolymer) appears to have adequate loss properties at microwave frequencies (Riddle *et al.*, 2003), is relatively cheap and easy to machine. Figure 13 shows that neither the Teflon nor the Delrin enclosures has any significant effect on the ranging accuracy or SNR of the system.

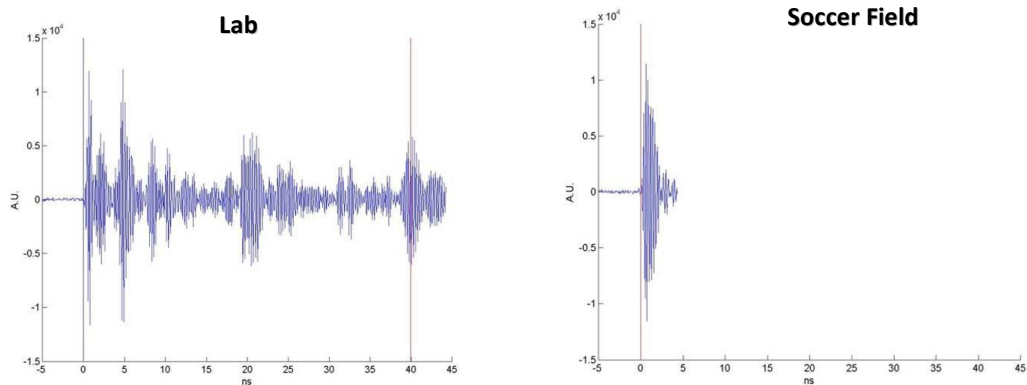


Figure 8. Received waveforms in both high and low multipath environments. These figures show the received waveforms stored on the transceiver. The left figure is the received waveform obtained in a laboratory setting with many reflective surfaces, several large rotating ceiling fans and people moving about. The right figure shows a waveform obtained in the soccer field, as shown in Figure 3. They are plotted on the same scale. The vertical axis is in arbitrary units returned by the transceiver and the horizontal axis is time from the estimated leading edge of the pulse, in nanoseconds. The red line represents the point at which the system first detects a pulse has arrived.

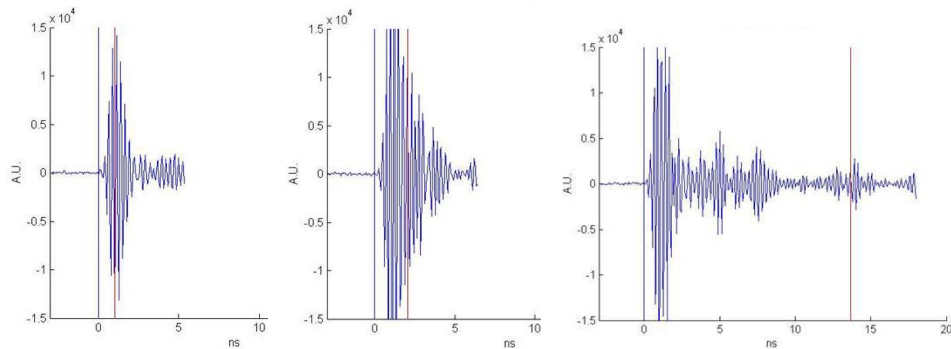


Figure 9. Received waveforms in a representative mining environment. In these measurements, each transceiver was mounted on a separate large vehicle in the Bracalba Quarry, Queensland. The three plots represent the variation of the relative orientation of the vehicles. Each plot shows a variation in this angle of 60° . The axes are as for Figure 8.



Figure 10. The experimental setup for measuring reflection effects. The image in the left shows the metal plate attached to the polycarbonate enclosure. In this case the lid is removed, allowing the phase centre of the antenna to be surveyed. The dimensions of the plate are 400×400 mm, which subtends an angle of approximately $\pm 53^\circ$ from the antenna. This represents approximately 75% of the useful beam pattern of the antenna, in elevation (Time Domain, 2011). Both transceivers were fitted with these plates and orientated such that the plates were as close to parallel as possible. The figure on the right shows the metal shroud mounted on the polycarbonate enclosure. In this image, the polycarbonate lid, the dark part of the enclosure, is mounted. The shroud covers five sides of the enclosure and was mounted on both transceivers.

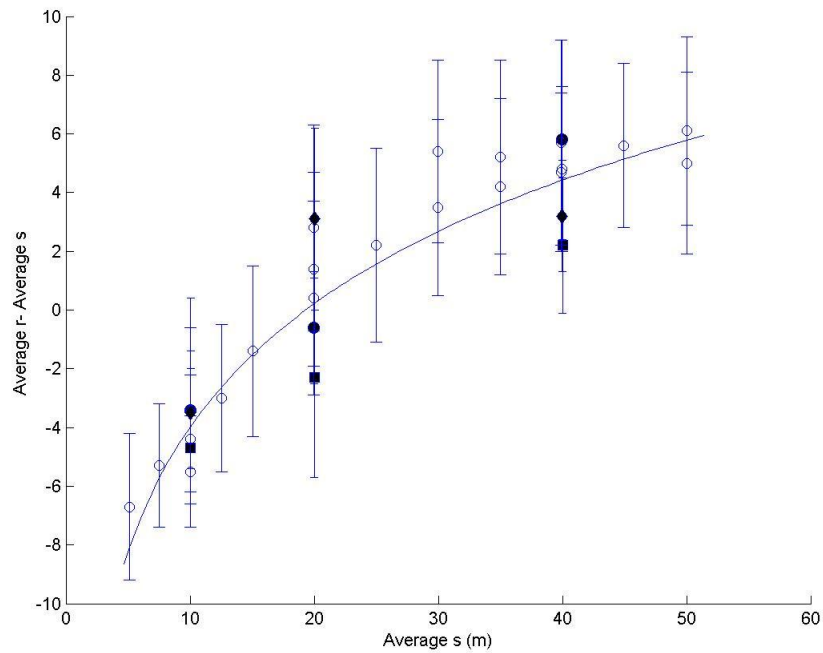


Figure 11. Measurements with reflectors and increased gain. This figure is the same as Figure 6 with the inclusion of measurements made with nearby reflectors and increased gain. The open circles are the data from Figure 6. The diamonds represent the data obtained with the metal plate, see Figure 10, and the squares represent the data measured with the metal shroud. The filled circles represent that data obtained when the amplifier gain of both transceivers were increased by approximately 7 dB. Higher gains caused saturation of the transceivers at short ranges, The gain and plate data points overlap at 10 m.

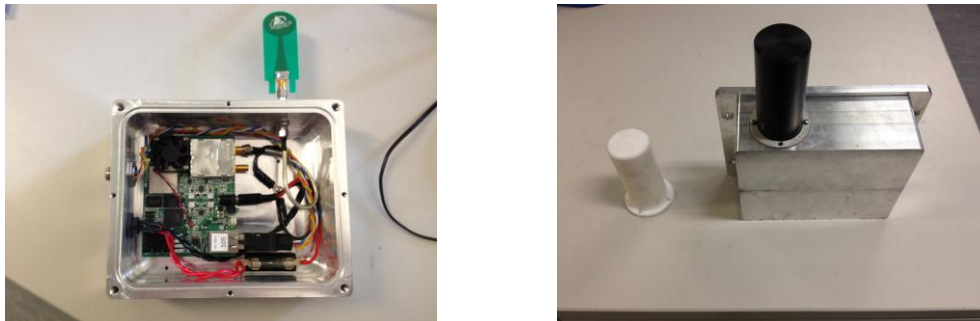


Figure 12. Hermetic enclosures for the transceiver. The enclosure is manufactured from 1 cm thick aluminium. The left figure shows the transceiver mounted within its enclosure. The antenna is mounted on a hermetic SMA feedthrough, which is connected to the transceiver by a short length of 141 hand-bendable coaxial cable. The left figure show the sealed unit with the separate antenna enclosure. The white enclosure next to the Al box is made of Teflon, and Delrin is the black, mounted on the box. Each has a wall thickness of 5 mm.

MEASUREMENTS WITH IMPROVED FIRMWARE

In May this year, Time Domain released a new version of their firmware. The manufacturers state that they had improved significantly their ranging algorithm and the measurement speed. We were among the first to acquire and test these improved devices.

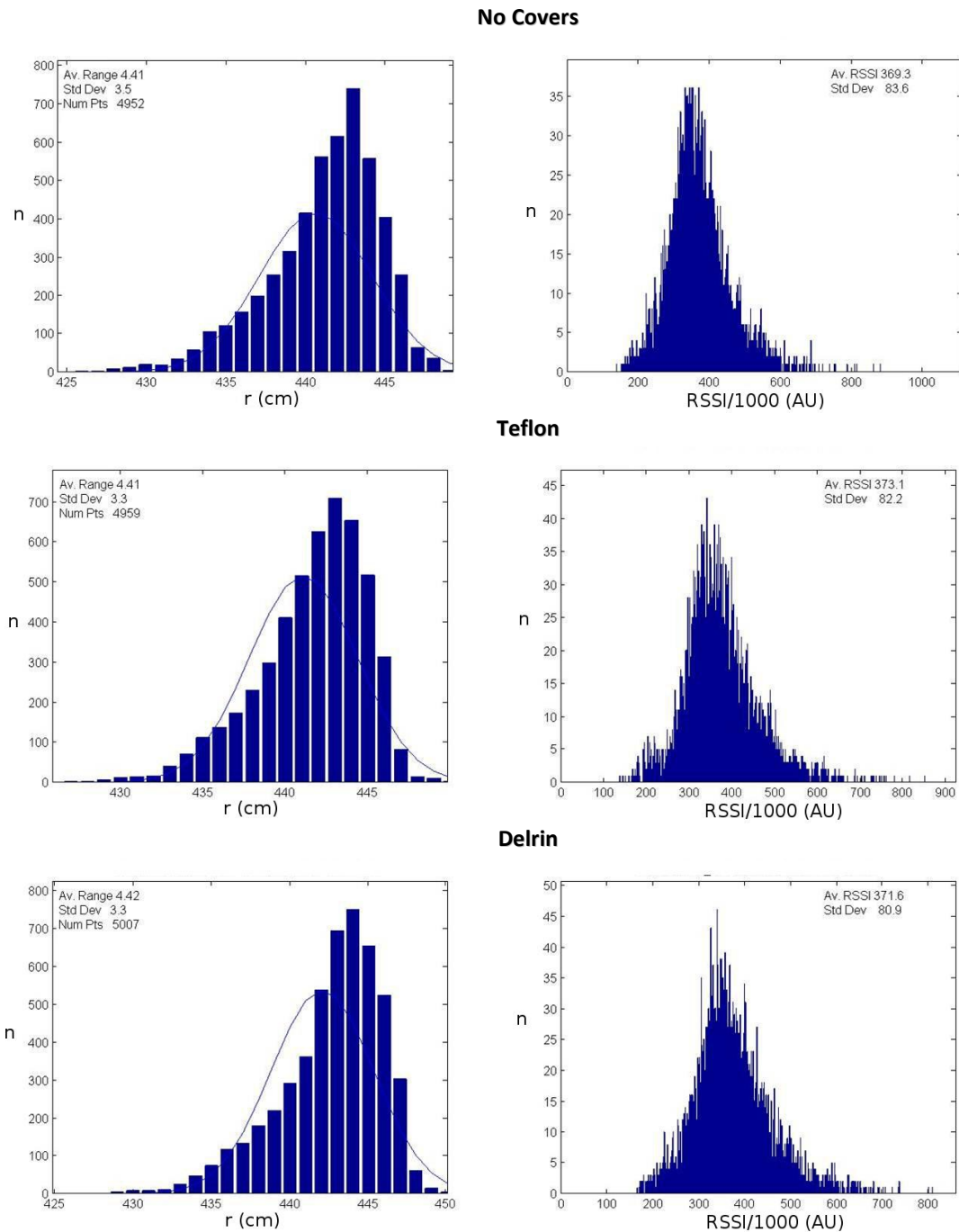


Figure 13. Ranging measurements with various antenna enclosures. These results were obtained in a laboratory environment. The left figures show the histograms of the ranging measurements, as for Figure 4. The figures on the right show the histograms of the Received Signal Strength Indicator (RSSI), as returned by the transceiver. The RSSI is a measure of the SNR of the individual range measurements. The measurements were made with both transceivers mounted in the AI enclosures, as in Figure 12. The results were obtained without any covers on either transceiver and with Teflon and Delrin covers on both antennas. Within the level that can be measured in the laboratory environment, there is no statistically significant variation in SNR between the results obtained without any covers at all and Teflon or Delrin covers for resolution, accuracy or SNR.

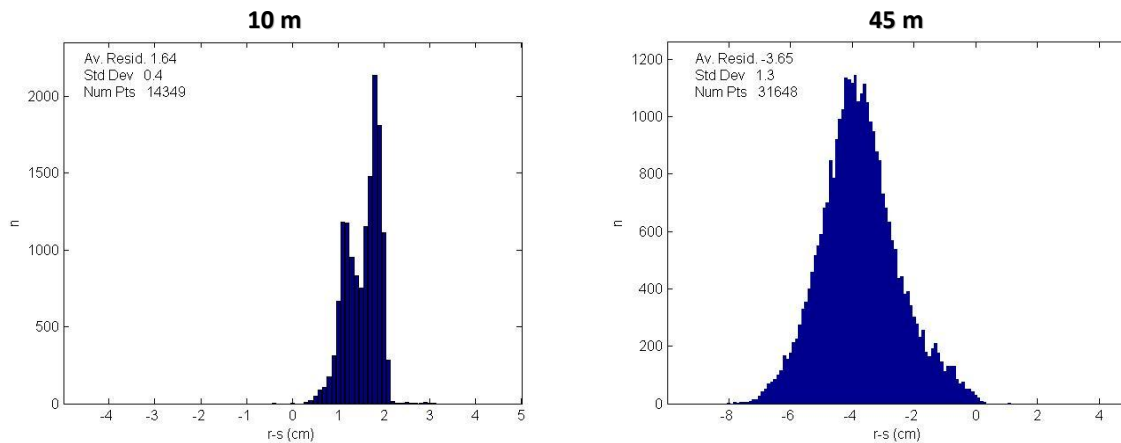


Figure 14. Resolution measurements at two ranges for transceivers with the new firmware. The figures show examples of the histograms of the difference between the range measured with the UWB transceivers, r , and that obtained by surveying, s . The figure on the left was obtained at 10 m, and the figure on the right was obtained at 45 m. The bin widths are 1 mm. The closer range has a standard deviation of only 4 mm, while even the relatively poor result at the longer range has a resolution of 1.3 cm.

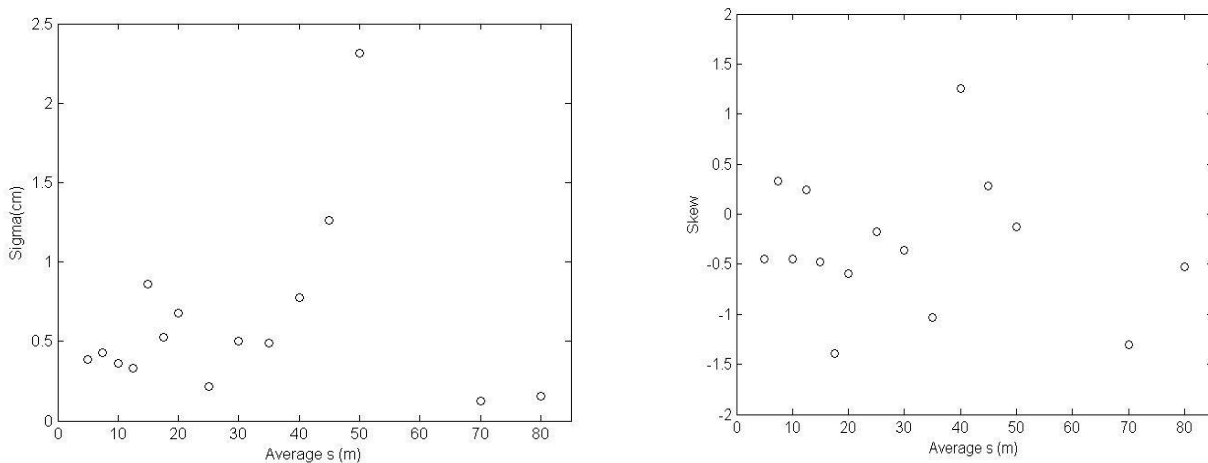


Figure 15. Summary of the range measurements at 15 ranges for transceivers with the new firmware. These figures have the same format as those presented in Figure 5, where s is the separation between the antennas, as measured by surveying.

Experimental Setup

We carried out measurements with a single pair of transceivers delivered from the factory with the new firmware, in an experimental setup similar to that shown in Figure 3. We used the same default configuration as previously, i.e. default gain and default antenna configuration. We carried out a series of measurements at 15 ranges from 5 to 80 m.

We measured the conversion time for averaging over 128 pulses as approximately 20 ms, a reduction by a factor of two over the previous measurements. For these measurements, we took data as fast as our custom software would allow. For averaging over 128, 64, and 32 pulses, we achieved acquisition rates of 46.7, 73.4 and 102 Hz, respectively. All the data we present here were obtained with averaging over 128 pulses.

Resolution

Figure 14 shows two examples of the histograms of the ranging measurements. It is immediately apparent that there is a marked improvement in resolution. The summary of the measurements at 15 ranges is shown in Figure 15. They show the resolution is better than 5 mm for ranges < 30 m. Even the worst resolution obtained at 50 m is comparable to the best resolution obtained with the original firmware.

Figure 15 also shows that the skewness is still present, but is not as large nor does it have the same systematic variation as seen previously.

Accuracy

Figure 16 shows the range bias for measurements carried out with the new firmware. There is a sharp discontinuity at 40 m. The existence of this discontinuity was confirmed by repeated measurements on separate days and moving the test to another part of the soccer field.

It is most likely that this discontinuity is due to the reflection from the ground between the two transceivers (Dewberry, 2012). The second Fresnel zone is the surface for which the path difference between the direct line of sight signal and the reflected waves off the surface is equal to one wavelength, λ . Due to the phase inversion from the reflection, a path difference of λ will cause destructive interference.

The centre frequency of the transceiver's bandpass is 4.2 GHz, corresponding to a wavelength of 7 cm. The wavelength is small with respect to the pulse length, approximately 30 cm. Therefore, a path difference of λ , will cause interference with the pulse. This would cause significant reduction in the SNR and may significantly distort the shape of the pulse. Given the total separation of the transceivers, D , it can be shown that the radius of the second Fresnel zone is approximated by (Rappaport, 2002):

$$r_{2f} = \sqrt{(\lambda D/2)} \quad . \quad 2$$

For $D = 40$ m and $\lambda = 7$ cm, $r_{2f} = 1.2$ m, which, rather unfortunately, corresponds to the typical height of the tripods we used during these measurements. We expect that increasing the height of the transceivers above the ground will significantly extend the range at which this discontinuity occurs, e.g. if $r_{2f} > 2$ m, $D > 110$ m.

At ranges less than 35 m, there does not appear to be any significant variation of the difference of the UWB measured range with respect to the surveyed range. It appears to be a constant offset of approximately 1.7 cm.

Nominally any constant offsets are removed by calibration at the factory. However, in this case it remains. Since these measurements, these transceivers have been mounted in the hermetic enclosures, see Figure 12, and they have been calibrated to remove the propagation delay of the coax cable between the antenna and the transceiver. Preliminary measurements indicate that the constant offsets present in Figure 16 have been removed.

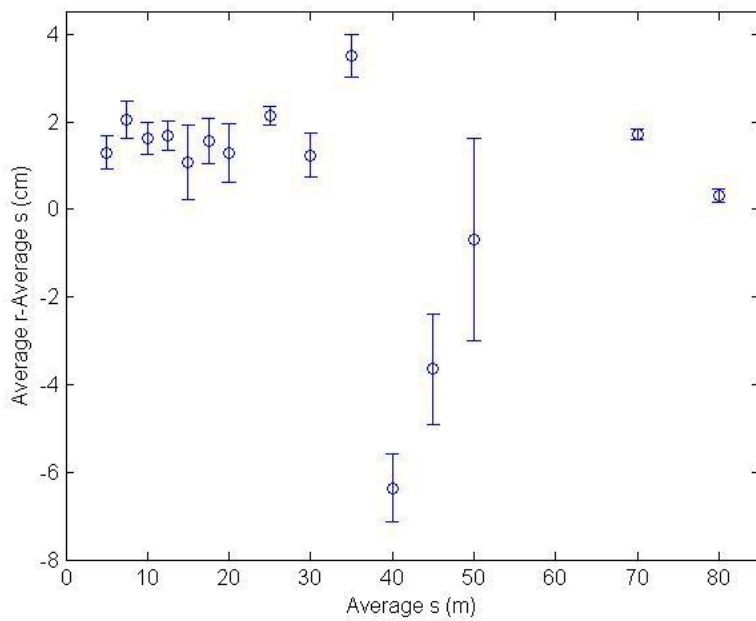


Figure 16. The range bias of the measured mean range with the new firmware. The format for this figure is the same as for Figure 6.

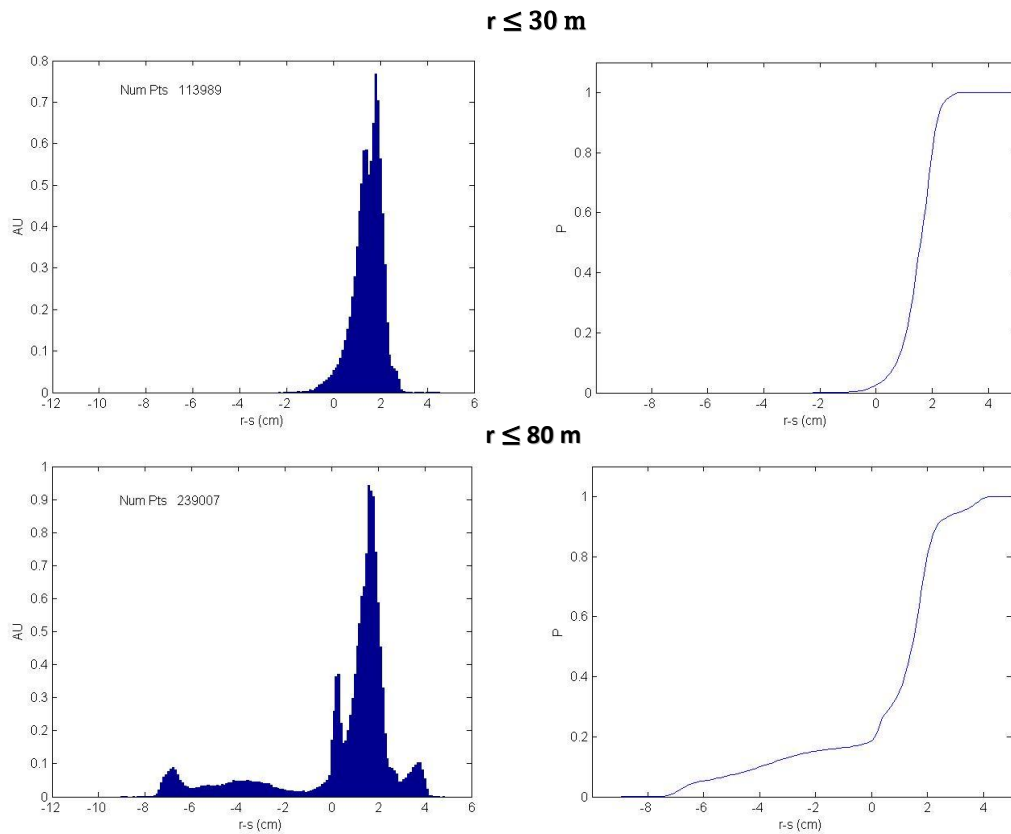


Figure 17. The merged histograms for the individual range measurements obtained with the new firmware. The top figures are the merged histogram and cumulative probability distribution for all of the range measurements up to 30 m. It represents approximately half of the total data. The lower figures are the merged histogram and cumulative probability distribution for all of the data, up to a range of 80 m. In these plots, the number of events at any given range has been normalized and the vertical axis is in arbitrary units. The horizontal axis is the same as for Figure 7.

The merged histograms of the range measurements are shown in Figure 17. For ranges up to 30 m the resolution is excellent. The centre of the cumulative probability distribution of the centre is at +1.7 cm, 90% of the measurements lie within ± 1 cm and 99% within ± 2 cm from the centre.

For ranges > 30 m, there is significant bias to shorter ranges all of which appear clustered around the discontinuity at 40 m. The centre of the cumulative probability distribution is at +1.5 cm, 86% lie within ± 4 cm and 96% lie between $- 8$ cm and $+ 4$ cm from the centre.

CONCLUSIONS

We have presented measurements characterizing the ranging performance for a commercial UWB transceiver. With the latest firmware upgrades, this system provides excellent resolution and accuracies at ranges < 30 m, resolution less than 5 mm and 99% of events within ± 2 cm. These results represent the best performance for a radio transceiver based ranging system presented in the literature that we are aware of. The resolution performance approaches that of laser surveying. At ranges from 30 to 80 m, the performance is still an improvement on results that other authors and ourselves have measured previously. The system provides reliable ranging performance even in close proximity to reflecting surfaces. In a mining environment, using care in the design of the transceiver mount, the only reflection that causes significant degradation of the system performance may be due to the ground, which may only occur at extremely long ranges. The excellent performance makes this system an ideal candidate for precision ranging in most mining applications.

ACKNOWLEDGEMENTS

We would like to acknowledge the support of CRCMining and ACARP grant C16031. We appreciate the assistance of Matthew Green and Tyson Philips for support during the measurements. We are also grateful to Brandon Dewberry and Jon Hedges from Time Domain for their help and advice.

REFERENCES

Cho, Y K, Youn, J H, and Martinez, D, (2010), *Error modelling for an untethered ultra- wideband system for construction indoor asset tracking*, Automation in Construction, **19**, pp. 43-54.

Dewberry, B, (2012), Time Domain Corporation, *private communication*.

Dewberry, B, and Beeler, W, (2012), *Increased Ranging Capacity using Ultrawideband Direct-path Pulse Signal Strength with Dynamic Recalibration*, presented at IEEE/ION Position and Location Symp., Myrtle Beach, SC, USA.

Gezici, S, Molisch, A F, Poor, H V, and Kobayashi, H, (2007), *The Trade-off between Processing Gains of an Impulse Radio UWB System in the presence of Timing Jitter*, IEEE Trans. Communications, **55**, pp. 1504-1515.

Goldhirsh, J, *Attenuation and Backscatter From a Derived Two-Dimensional Duststorm Model*, (2001), IEEE Trans. Antennas Propagation, **49**, pp. 1703-1711.

Kay S. M., (1993), *Fundamentals of Statistical Signal Processing, Vol. 1 Estimation Theory*, Prentice Hall, Upper Saddle River, N. J., USA.

Maxim (2003), *An Introduction to Spread Spectrum Communications*, Maxim Application Note, **1890**, Maxim Intergrated Products, Sunnyvale, CA, USA, www.maxim-ic.com/an1890

McGougan, G D, (2009) *Real-Time Kinematic Surveying using Tightly-Coupled GPS and Ultra-Wideband Ranging*, Ph.D. Thesis, University of Calgary, Canada, UCGE Reports, **20293**.

Miller, L E, (2003), *Why UWB? A Review of Ultrawideband Technologies. Report to NETEX Project Office, DARPA, NIST*, www.antd.nist.gov/wctg/manet/NIST_UWB_Report_April03.pdf

Molisch A F, (2006), *Introduction to UWB Signals and Systems*, in *Ultra Wideband: Antennas and Propagation for Communications, Radar and Imaging*, Okon E, Allen, B, Malik, W, Edwards D and Brown A K, eds., Wiley, New York, USA.

Nakagawa, T, Ono, G, Fuliwara, R, Norimatsu, T, Terada T, Mizugaki, K, and Miyazaki, M, (2009), *UWB IR Transceivers for Simultaneous Data Communications and Accurate Localization*, presented at CMOS Emerging Technologies Workshop, Vancouver, B.C., Canada.

Nanotron Technologies GmbH, White Paper, (2007), *nanoNET Chirp Based Wireless Based Networks*, Nanotron Technologies GmbH, Alt-Moabit 60, 10555 Berlin, Germany.

Nanotron Technologies GmbH, (2011), Alt-Moabit 60, 10555 Berlin, Germany. www.nanotron.com

Olsen, R L, Rogers, D V, and Hodge, D B, (1978), *The aR^b Relation in the Calculation of Rain Attenuation*, IEEE Trans. Antennas Propagation, **26**, pp. 318-329.

Park, J, Demaine, E D, and Reller, S., (2008) *Moving Baseline Localization*, IEEE 2008 Int. Conf. on Information Processing in Sensor Networks, St. Louis, Mo, USA, pp. 15-26.

Rappaport, T S, (2002), *Wireless Communications: Principles and Practice*, Prentice Hall, Upper Saddle River, N. J., USA.

Richardson, P, and Shan, D, (2009), *Experimental Data Collection and Performance Analysis of Outdoor UWB Positioning System under Static and Mobile Conditions*, EURASIP J. Wireless Communications, **2009**, 2009:618036.

Riddle, B, Baker-Jarvis, J, and Krupka, J., (2003), *Complex permittivity of Common Plastics Over Variable Temperatures*, IEEE Trans. Microwave Theory Tech., 51, pp. 727-733.

Rommel, A, and Haich, R, (2009), *RTLS Architectures in Theory and in Practice*, presented at Wireless Congress, Munich, Germany.

Schantz, H G, (2003), *Bottom Fed Planar Elliptical UWB Antennas*, Proc.. IEEE Ultra Wideband Sys. Technol. Conf., Reston, Va, USA, pp. 219-223.

Sahinoglu, Z, Gezici, S, and Guvenc, I, (2008), *Ultra-wideband Positioning Systems, Theoretical Limits, Ranging Algorithms, and Protocols*, Cambridge University Press, Cambridge, U.K.

Time Domain, (2011), *Data Sheet, PulsON 400 RCM, Data Sheet, BroadSpec UWB Antenna, PulsON 400 Ranging & Communications Part Two: UWB Definitions and Advantages*, Time Domain Corporation, Cummings Research Park, 4955 Corporate Drive, Suite 101, Huntsville, AL 35805, USA.

www.timedomain.com/datasheets/320-0289BP400RCMDataSheetFinal.pdf

www.timedomain.com/datasheets/TD_BroadSpec_Antenna.pdf

www.timedomain.com/datasheets/320-0291B Part Two UWB Definition & Advantages.pdf

Ubisense Ltd, (2012) St Andrew's House, St. Andrew's Road, Chesterton, Cambridge, CB4 1DL, UK. www.ubisense.net

Zebra Technologies Corporation, (2011), 475 Halfday Rd, Suite 500, Lincolnshire, Ill, 60069, USA. www.zebra.com

Zhang, C, Hammad, A, and Rodriguez S, (2011), *Crane Pose Estimation Using UWB Real-Time Location System*, to appear J. Comput.Civ. Eng.